Langmuir

Article

pubs.acs.org/Langmuir

Surface Pressure Isotherm for a Monolayer of Charged Colloidal Particles at a Water/Nonpolar-Fluid Interface: Experiment and Theoretical Model

Plamen V. Petkov, Krassimir D. Danov, and Peter A. Kralchevsky*

Department of Chemical Engineering, Faculty of Chemistry and Pharmacy, Sofia University, 1164 Sofia, Bulgaria

Supporting Information

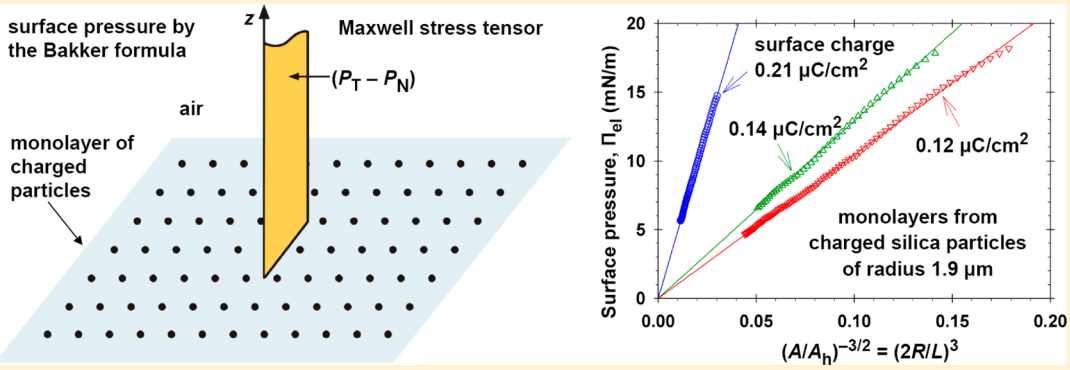

ABSTRACT: Monolayers from electrically charged micrometer-sized silica particles, spread on the air/water interface, are investigated. Because of the electrostatic repulsion, the distances between the particles are considerably greater than their diameters, i.e., we are dealing with nondensely packed interfacial layers. The electrostatic repulsion between the particles occurs through the air phase. Surface pressure vs area isotherms were measured by Langmuir trough, and the monolayers' morphology was monitored by microscope. The mean area per particle is determined by Delaunay triangulation and Voronoi diagrams. In terms of mean area, the surface pressure for monolayers from polydisperse and monodisperse particles obeys the same law. The experiments show that $\Pi \propto L^{-3}$ at large L, where Π is the surface pressure and L is the mean interparticle distance. A theoretical cell model is developed, which predicts not only the aforementioned asymptotic law but also the whole $\Pi(L)$ dependence. The model presumes a periodic distribution of the surface charge density, which induces a corresponding electric field in the air phase. Then, the Maxwell pressure tensor of the electric field in the air phase is calculated and integrated according to the Bakker's formula to determine the surface pressure. Thus, all collective effects from the electrostatic interparticle interactions are taken into account as well as the effects from the particle finite size. By evaporation of water, the particle monolayers are deposited on a solid substrate placed on the bottom of the trough. The electrostatic interparticle repulsion is strong enough to withstand the attractive lateral capillary immersion forces that are operative during the drying of the monolayer on the substrate. The obtained experimental results and the developed theoretical model can be useful for prediction and control of the properties of nondensely packed interfacial monolayers from charged particles that find applications for producing micropatterned surfaces.

1. INTRODUCTION

The electrostatic repulsion in monolayers of charged micrometer-sized particles on an air/water or oil/water interface leads to interparticle distances which are considerably greater than particle diameters,[1−3] i.e., we are dealing with nondensely packed colloidal layers.[4] During the past decade, such monolayers have been investigated in view of their use for producing micropatterned surfaces with applications for antireflective and superhydrophobic coatings,[4−6] microlens arrays,[7,8] and structures in biosensing and bioengineering,[9,10] in relation to their importance for the interactions in Pickering emulsions,[11−14] and for phase-transfer catalysis.[15,16]

The first surface-pressure measurements with nondensely packed interfacial monolayers have been carried out with latex particles.[1−3] Aveyard et al.[3] derived an analytic formula for the electrostatic surface pressure vs trough area, which agrees well with experimental data over a wide range of surface pressures. In subsequent studies with laser tweezers it was established that the electrostatic interparticle forces obey the law of dipole−dipole interactions throughout the nonpolar fluid (oil, air).[17] This interaction can be due to charges located at both the particle/nonpolar-fluid[17] the and particle/water[18] interfaces. Nondensely packed particle monolayers have been investigated at oil/water[19,20] and air/water[4,21] interfaces. The effect of applied external electric field on the monolayer's morphology[22] and instabilities due to collective effects engendered by long-

Received: January 10, 2014
Revised: February 21, 2014
Published: February 24, 2014

   dx.doi.org/10.1021/la500126d | Langmuir 2014, 30, 2768−2778

range capillary forces[23,24] have been also studied. The particle monolayer could be transferred onto a solid substrate via the vertical Langmuir−Blodgett deposition or the horizontal Langmuir−Schaeffer deposition.[25,26] To prevent damaging of the nondensely packed layer by the lateral capillary forces, a horizontal deposition on a substrate covered by an adhesive polymer layer was used.[27]

Our first goal in the present study was to investigate whether the surface pressure isotherm, $\Pi(\alpha)$ (with α being the surface area per particle), obeys the same law for monodisperse and polydisperse charged particles. For polydisperse particles, α can be determined as an average value by Delaunay triangulation and construction of Voronoi diagrams.[28] The results showed that the $\Pi(\alpha)$ dependences are really similar for polydisperse and monodisperse particles. In both cases, the surface pressure exhibits a wide asymptotic region with $\Pi \propto L^{-3}$ (at large L), where $L \equiv \alpha^{1/2}$ is the characteristic interparticle distance within the monolayer. The only available theoretical model[3] for the surface pressure of a monolayer from charged particles asymptotically predicts a different power law, viz. $\Pi \propto L^{-5}$ at large L. Thus, our next goal was to construct a theoretical model which yields an asymptotic dependence $\Pi \propto L^{-3}$, in agreement with the experiment. The obtained $\Pi(L)$ dependence describes very well the experimental surface pressure isotherms at all interparticle separations, not only at large L.

Deposition of the produced nondensely packed interfacial monolayers on a solid plate has been also attempted. The intriguing point is whether the electrostatic repulsion between the particles is strong enough to withstand the powerful attractive lateral capillary immersion force that appears upon the particle confinement in a liquid film on the substrate.[29] The results from the measurements are reported and discussed in section 3, whereas the theoretical model is developed and tested against experimental data in section 4.

2. MATERIALS, METHODS, AND PROCEDURES

2.1. Preparation of Electrically Charged Particles. In our experiments, we used silica particles Excelica UF305 produced by Tokuyama Corp., Japan, by melting of synthetic SiO_2. The particles were spherical but polydisperse. During the cleaning procedure (see below), the smallest Brownian particles were removed. The diameters of 7300 particles spread on the air/water interface were measured. Following a procedure described elsewhere,[30] the experimental cumulative function was fitted with the log-normal distribution. The curve corresponding to the best fit is shown in Figure 1a. The maximum corresponds to R_p = 1.92 μm. The radii of 50% of the particles belong to the interval $1.56 \le R \le 2.37$ μm; for details, see eq S1, Supporting Information, and the related text in Appendix A, Supporting Information.

Before an experiment, the particle surfaces were cleaned following procedures proposed elsewhere.[31,32] First, the particles were placed in sulfochromic acid for 2 h. Next, they were abundantly rinsed with water. The particles were separated from the water by centrifugation at 5000 rpm for 3 min. The rinsing was repeated three times. Next, the particles were placed in 0.01 M NaOH solution for 6 h. Afterward, they were rinsed with deionized water and left for 40 min to sediment. Further, the water phase was removed together with the smallest (Brownian) particles. Finally, the particles were dried for 16 h at 80 °C.

The particles were hydrophobized by the following procedure:[19,33] 1 g of the cleaned and dried particles was placed in 30 g of a solution of dichlorodimethylsilane (DCDMS, 99.5%, Fluka) in cyclohexane. The closed glass beaker with solution + particles was sonicated in an ultrasonic bath. This was executed for 40 min as a cyclic process: (i) sonication until the temperature of the water bath reached 40 °C followed by (ii) ceasing of sonication and cooling to room temperature, etc. Further, the particles were rinsed once with pure cyclohexane, twice with chloroform, and, finally, once with absolute alcohol. The rinsing with a given solvent includes 15 min treatment in an ultrasonic bath, followed by centrifugation to separate the particles from the serum. After the last rinsing, the particles were first dried in a vacuum drier and next for 40 min at 110 °C. If such dried particles are placed on the surface of water, they repel each other as visible from the considerable distances between them. By placing a needle-shaped electrode above the monolayer, we established that the particles are negatively charged. A possible reason for these surface charges could be adsorption of ions from the air on the particles during drying. It is known that the air contains 200−800 negative ions per cm^3 at normal fair weather.[34]

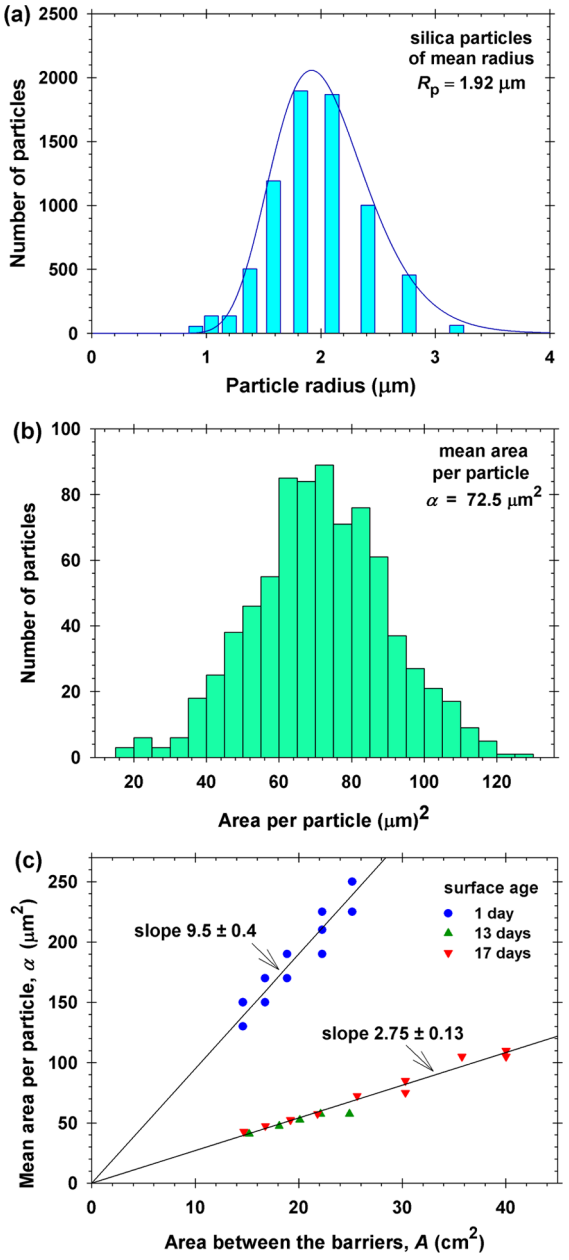

Figure 1. (a) Size distribution of the used particles and its fit with a log-normal distribution—the solid line. (b) Illustrative size distribution of the areas per particle at a given degree of compression for particles of surface age 17 days. (c) Plot of the determined mean area per particle, α, vs the area between the barriers, A, for particles of three different surface ages denoted in the figure.

dx.doi.org/10.1021/la500126d | Langmuir 2014, 30, 2768−2778

The prepared charged particles were stored in a closed beaker with 20 mL of isopropyl alcohol (IPA). The storage time is cited below as *surface age* of the particles. Before each experiment, the glass beaker with the particle suspension in IPA was sonicated in a water bath. Afterward, a portion of the suspension was taken with a pipet and spread on the surface of water in the Langmuir trough. The IPA evaporates, and a particle monolayer is deposited on the water surface.

To estimate the particle *contact angle*, we carried out experiments with water drops on finely polished flat plates of fused quartz—the same material as that of the particles. The plates were subjected to the same procedure of cleaning and hydrophobization as the particles. The air/water/plate contact angle was measured with drops from deionized water deposited on the substrate by a vertical syringe using the drop-shape method with an apparatus DSA30 (Krüss GmbH). The average contact angle, determined from 10 independent runs, was 85.4° ± 1.5°.

Using silica particles hydrophobized by the same procedure, it has been established[19] that the interparticle repulsion is insensitive to whether the dried particles are placed on the surface of deionized water or on 1 M NaCl solution. This result means that the electric field is created by charges at the particle/nonpolar fluid interface. An analogous experiment was carried out with our hydrophobized particles. First, the particles were spread on the surface of deionized water and $\Pi(A)$ isotherms were measured (A is the surface area). Next, with the help of two syringes the water was replaced with 100 mM aqueous NaCl solution and $\Pi(A)$ isotherms were measured again, with the *same* particle monolayer. Interestingly, the data indicate that Π is greater when NaCl is present in the water phase; see Figure S9 in Appendix A, Supporting Information. This is exactly the opposite of the effect that should be observed if the electric field is due to surface charges at the particle/water interface. A possible explanation of the observed effect can be that the particle contact angle is greater in the presence of NaCl, i.e., that the hydrophobic particles experience a "salting out" effect, so that the area of the particle/air interface (and the total charge on this interface) increases. This effect deserves a special investigation, which is out of the scope of the present study. Here, it is important only that the electric field is created by charges at the particle/air interface, as in ref 19.

2.2. Particle Monolayers in a Langmuir Trough. In our experiments, a KSV NIMA Minimicro Langmuir trough was used. The particle monolayers formed in the trough were observed from below (through a glass window in the bottom of the trough) by an inverted microscope Axiovert 40 MAT (Carl Zeiss). The inner dimensions of the trough are 195 × 51 × 4 mm, with a maximal distance of 170 mm between the two barriers. The whole setup was mounted on an active vibration isolation system TS-150 and closed in a container with transparent walls to avoid contaminations from the air. The surface pressure, Π, was measured using the Wilhelmy plate method.

The trough was filled with a layer of deionized water of 3 mm thickness. The experiments begin if the initial surface pressure is $\Pi <$ 0.5 mN/m. The initial area between the barriers was 40 cm^2. Before each experiment, the suspension of silica particles in isopropyl alcohol was dispersed by sonication. Next, several drops of the suspension were placed on the water surface between the barriers of the trough. The number of drops was 5 for particles of surface age $\leq$ 5 days (of greater charge), whereas the number of drops was 12 for particles of age >10 days (of smaller charge). After placing the particles on the water surface, we waited for 1−2 h until a stable value of Π is established. Next, the variation of Π was recorded during several cycles of continuous compression/expansion of the particle monolayer at rates of 0.017 and 0.05 cm^2/min. (These low rates are due to the use of a mini-trough.) No effect of the compression/expansion rate on the surface pressure isotherm was observed, in agreement with ref 26, where no effect was detected even at much higher rates, in the range from 10 to 814 cm^2/min. One of the compressions was carried out in a stepwise manner. At each step, different parts of the monolayer were recorded by a video camera at fixed distance between the barriers. The working temperature was 25 °C.

2.3. Determining the Mean Area Per Particle by Processing of Video Frames. From the video records, the average area per particle in the monolayer, α, was determined at different stages of compression, characterized by the total area between the barriers, A. For this goal, the size distribution of the areas per particles was determined (see Figure 1b), and α was calculated as an arithmetic mean value. The data for α were plotted vs A (Figure 1c) to verify whether the number of particles at the interface is constant during compression of the monolayer, i.e., whether particles do not desorb in the subphase upon compression, which has been observed by other authors.[35]

Figure 2a shows a typical video frame of a particle monolayer, which has been obtained at compression to surface area A = 25.6 cm^2 for a suspension of surface age 17 days. The processing of the video frames was carried out using the functions Delaunay triangulation, convex hull, Voronoi diagram, and bounded diagram from the computational geometry package of Wolfram Research, Inc., Mathematika, Version 8.0, Champaign, IL (2010). First, the centers of all particles were determined and the centers of all neighboring particles were connected. Thus, the plane is covered with a set of triangles (Figure 2b). Further, the centers of the circumscribed circles of all neighboring triangles are connected with segments (Delaunay triangulation), and in this way, each separate particle is surrounded by a polygon (Voronoi cell), i.e., a Voronoi diagram is constructed;[28] see Figure 2c. The

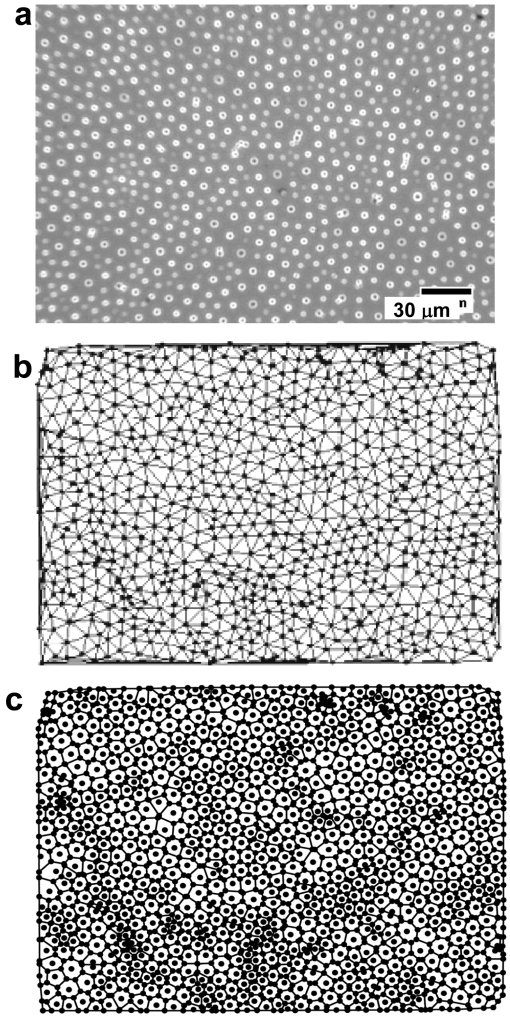

Figure 2. Illustration of the procedure for computer processing of video frames. (a) Photograph of a given portion of the monolayer. (b) Centers of the neighboring particles are connected (Delaunay triangulation). (c) Voronoi diagram is constructed; area of the polygon surrounding each particle is identified with the respective area per particle.

dx.doi.org/10.1021/la500126d | *Langmuir* 2014, 30, 2768−2778

surface area that belongs to a given particle is identified with the area of the Voronoi cell for this particle. The size distribution of the areas of all cells in Figure 2c is shown in Figure 1b. Finally, by calculating the mean arithmetic of this distribution, we determine the mean area per particle, α, for the respective video frame.

2.4. Deposition of a Nondensely Packed Particle Monolayer on a Solid Plate. In these experiments, a circular silica plate of diameter 30 mm and thickness 3 mm was placed on the bottom of the Langmuir trough. Next, deionized water was poured in the trough to form an aqueous layer of thickness 4 mm. Thus, the thickness of the water layer above the plate is 1 mm. Further, a monolayer of particles is spread on the air/water interface, as described above. The monolayer is compressed to a given area between the barriers, corresponding to a certain mean distance between the charged particles. During the evaporation of water from the trough, the monolayer's behavior is recorded by video camera connected to the microscope. After a certain period of time (which is about 2 h for evaporation in the atmospheric air at a temperature of 27 °C), the particle monolayer is deposited on the surface of the solid plate. The video record of the whole process shows whether the structure of the initial nondensely packed monolayer is preserved after its deposition on the plate (after its complete drying) and how large are the changes in the interparticle distances, if any.

3. EXPERIMENTAL RESULTS AND DISCUSSION

3.1. Mean Area Per Particle vs the Degree of Compression. As illustrated in Figure 1b, the distribution of the areas per particle is symmetric, close to Gaussian. For this histogram, which is obtained with particles of surface age 17 days (of relatively low surface charge), the mean area is 72.5 μm^2, which is considerably greater than the mean area of the particle equatorial cross-section, 11.6 μm^2. In other words, even for the investigated particles of lower surface charge we are dealing with nondensely packed interfacial monolayers. Additional photographs, Voronoi diagrams, and histograms corresponding to different degrees of compression of a given monolayer are shown in Figures S1−S3 in Appendix A, Supporting Information.

In Figure 1c, each experimental point represents the value of the mean area per particle, α, determined by processing of a given video frame using the procedure illustrated in Figure 2. As seen in Figure 1c, the data comply well with straight lines through the coordinate origin. The data for the particles of surface age 13 and 17 days can be fitted with the same line.

The relation between A and α is simple, viz. $A = N\alpha$, where N is the total number of particles contained in the monolayer confined between the barriers of the Langmuir trough. Thus, from the slopes of the upper and lower lines in Figure 1c we determine N = 10.6 and 36.4 million particles, respectively. The constancy of the slope for a given line means that the total number of particles, N, remains constant during compression of the monolayer, i.e., particles are not forced out in the aqueous subphase. This is fulfilled for all experimental data reported in this article.

We avoided experiments at higher degrees of compression, for which the $\Pi(A)$ isotherms obtained in different compression/expansion cycles with the same monolayer become irreproducible, which could mean occurrence of irreversible aggregation or particle desorption.

The scattering of the data around the straight line is greater for the particles of 1 day surface age in Figure 1c. This could be explained with a greater polydispersity of the particle electric charges. The particle charging seems to be an essentially stochastic process.

The characteristic distance between the particles $L = \alpha^{1/2}$ varies in the range $6.5 \le L \le 10.5$ μm for the lower line in Figure 1c and in the range $11.4 \le L \le 15.8$ μm for the upper line in the same figure. All these interparticle distances are considerably greater than the Debye screening length in the aqueous phase, which is κ^{-1} = 0.961 μm for pure water and κ^{-1} = 0.203 μm for water equilibrated with the atmospheric CO_2, which is the case of our experiments. These facts unambiguously indicate that we are dealing with interparticle repulsion across the nonpolar fluid (air, oil), as first established by Aveyard et al.,[3,17] and confirmed in a number of subsequent studies.[18−21]

3.2. Surface Pressure Isotherms. A typical surface pressure isotherm, Π vs A, is shown in Figure 3a for a compression/expansion cycle. To illustrate the experimental reproducibility, two such compression/expansion isotherms obtained with the same monolayer are compared in Figure 3b. The experimental curves are reproducible, although there is a weak tendency for the curves obtained upon expansion to lie slightly lower than those obtained upon compression. The separate points in Figure 3b correspond to processed video frames, from which the coefficient $N = A/\alpha$ (for conversion of the area between the barriers, A, into mean area per particle, α) is determined; see the previous subsection. Once determined, this coefficient is used to convert the experimental $\Pi(A)$ curves, obtained by continuous compression or expansion of a given monolayer, into $\Pi(\alpha)$ dependencies.

At the greatest expansions (lowest Π), the experimental $\Pi(\alpha)$ dependences are very slant. This could be explained with the fact that the electrostatic interaction has a certain range, so that above a given distance between the particles they are not strongly interacting and, thus, only a "gas" phase of particles is present. Our study is focused on the steep part of the surface pressure isotherm. The slant part is taken into account by an additive constant, Π_0, in the $\Pi(\alpha)$ dependence (see below).

In Figure 3b, the surface pressure is plotted vs $\alpha^{-3/2}$, because we established that in this scale the experimental curves are transformed into straight lines

$$\Pi = C\alpha^{-3/2} - \Pi_0 \tag{1}$$

where the coefficient C characterizes the slope of the experimental lines and Π_0 is a background surface pressure (see above). We found that at not so high compressions the experimental surface pressure curves obtained by Vermant et al.[20] also follow a linear dependence when plotted vs $\alpha^{-3/2}$; see Figure 3c. As shown in Figure S4 in Appendix A, Supporting Information, the same is true for the data by Aveyard et al.,[3] but in this case the region with linear dependence is narrower. These data have been obtained with monolayers from monodisperse polystyrene latex particles of radius R_p = 1.3 μm on a octane/water interface[3] and R_p = 1.55 μm on a decane/water interface.[20] The area of the monolayer, A, has been scaled with its value at close packing, $A_h = 2\sqrt{3}R_p^2N$ (hexagonal lattice), which is identified with the experimental value of A at the onset of monolayer's collapse.[3] Having in mind that $N = A/\alpha$, we obtain the relation between the scales on the horizontal axes in Figure 3b and 3c

$$A/A_h = \alpha/(2\sqrt{3}R_p^2) \tag{2}$$

Thus, linearization of the experimental curves in Figure 3b (polydisperse particles) and 3c (monodisperse particles) indicates that in both cases the same asymptotic law, eq 1,

dx.doi.org/10.1021/la500126d | Langmuir 2014, 30, 2768−2778

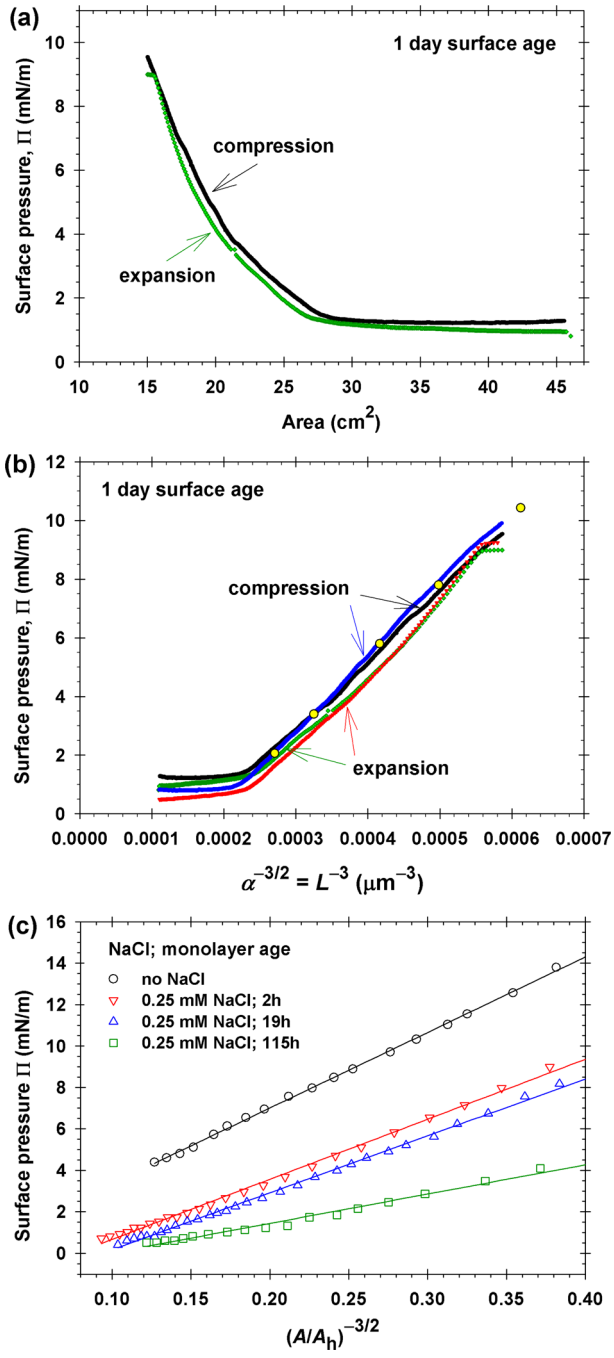

Figure 3. (a) Plot of our data for the surface pressure, Π, vs the area, A, for one compression/expansion cycle. (b) Plot of Π vs $\alpha^{-3/2}$ for two compression/expansion cycles, where α is determined from A using the calibration lines in Figure 1c (1 day surface age). Points correspond to photographs used to determine the calibration line. (c) Plot of Π vs $(A/A_h)^{-3/2}$ for data from ref 20; A_h is the value of A at close packing, just before the collapse.

holds. Theoretical interpretation of this result is given in section 4.4.

3.3. Results for the Monolayer Deposition on a Solid Plate. As described in section 2.4, the plate was laid on the bottom of the Langmuir trough, 1 mm below the particle monolayer at the air−water interface. Evaporation of water leads to a gradual decrease of the distance between the monolayer and the substrate. During the whole process, the monolayer is observed by optical microscope.

For the experiment documented in Figure 4, particles of surface age 13 days were spread on the air/water interface and

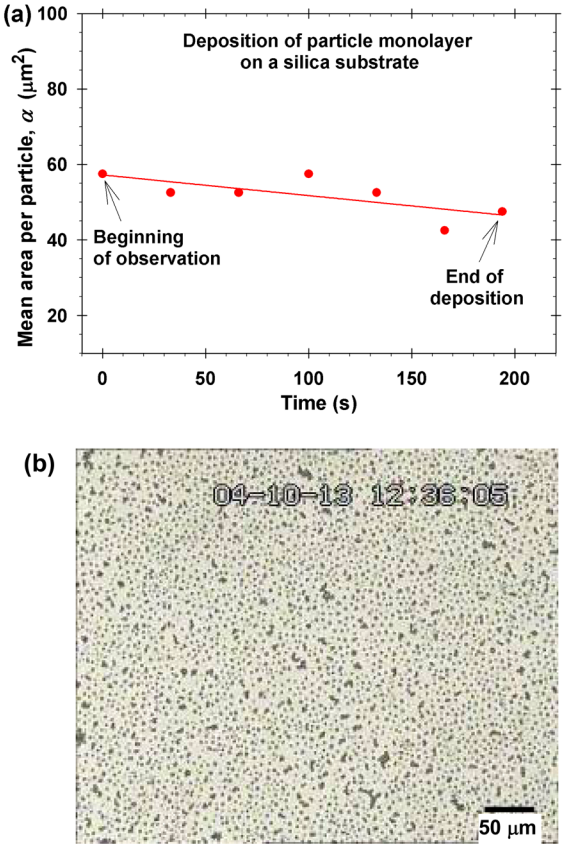

Figure 4. (a) Plot of the mean area per particle, α, vs time during the drying of a nondensely packed monolayer deposited on a planar substrate by evaporation of the solvent. Observations begin after the first changes are observed in the monolayer when the biggest particles are touching the substrate. (b) Photograph of a portion from the obtained dry particle monolayer deposited on the substrate.

the monolayer was compressed from 40 to 23.5 cm^2 area. At that, the initial mean area per particle was α = 57.5 μm^2. Initially, during evaporation of water no changes were observed in the monolayer. Small changes in the particle positions began 2 h 15 min after the start of the experiment when, supposedly, the bottoms of the bigger particles touched the substrate. These changes continued 3 min until complete drying of the particle monolayer on the substrate, but they were relatively small, so that the only way to quantify them was to process video frames of the process and determine the variations in α from the Voronoi diagrams, as described in section 2.3. Results are shown in Figure 4a. The data show that during the drying of the monolayer on the substrate, α decreases from 57.5 to 47.5 μm^2 (a shrinking of ~17%), which corresponds to a decrease in the characteristic distance L from 7.6 to 6.9 μm. This shrinking of the monolayer can be explained with the action of the attractive capillary immersion forces.[29] At this, the overall morphology of the layer is preserved, excluding the appearance of small clusters around some of the bigger particles—see the photograph of the dried monolayer on the substrate in Figure 4b; see also Figures S6 and S7 in Appendix A, Supporting Information.

Using the same software, from the Delaunay triangulation we determined the number of neighbors of each particle on video

dx.doi.org/10.1021/la500126d | Langmuir 2014, 30, 2768−2778

frames taken before and after deposition—see the histogram in Figure S8 in Appendix A, Supporting Information. The particles with six neighbors were 43.9% before deposition and became 42.5% after deposition. This difference is in the framework of the statistical scattering of the data. The results do not indicate any significant change in the degree of particle ordering during deposition.

The result of this experiment shows that *nondensely* packed layers of particles can be successfully deposited by evaporation of the solvent, as described above. The essential part of the deposition (when the thickness of the water layer is smaller than the particle diameters) takes about 3 min. The electrostatic repulsion between the particles is strong enough to preserve the monolayers morphology, despite the hydrodynamic drag forces accompanying evaporation of water and the lateral capillary attraction. If electrostatic interparticle repulsion was missing, the capillary forces would lead to formation of domains of densely packed particle monolayer, as observed in the process of convective self-assembly.[36]

4. THEORETICAL MODEL

4.1. Preliminary Discussion. Let us consider a charged colloidal sphere attached to the water/nonpolar-fluid interface. (The nonpolar fluid could be air or oil.) Because of the boundary conditions, the electric field in the nonpolar fluid asymptotically behaves as a field of a dipole. Charges at both the particle/water and particle/nonpolar-fluid interfaces can contribute to the effective dipole moment.[3,18,37−39]

The dipolar asymptotics of the field makes it possible to model the particle as a pair of electric charges separated at a finite distance (the particle charge and its mirror image with respect to the interface).[3] The superposition of the forces of interaction of a given particle-dipole with all other dipoles in the half-plane makes it possible to derive an analytical formula for the net electric force per unit length of the edge of the half-plane, i.e., for the surface pressure Π.[3] This approach to the calculation of Π yields $\Pi \propto L^{-5}$ at large L. However, the linear dependencies in Figure 3b and 3c indicate that at large α the experiment gives $\Pi \propto \alpha^{-3/2} = L^{-3}$. For this reason, we tried different versions of a theoretical model in order to achieve agreement with the experiment. A cell model with a periodic surface charge density (rather than discrete dipoles) that yields the experimental asymptotic relation, eq 1, is described below.

4.2. Model with Periodic Surface Charge Density. To take into account all collective effects that contribute to the value of Π, let us model the monolayer of charged particles as an interface with a periodic surface charge density (Figure 5a). The xy plane of the Cartesian coordinate system is chosen to coincide with the interface, whereas the z axis is perpendicular to it. The contribution of the electric field to the surface pressure, Π_{el}, can be calculated using the Bakker formula[40]

$$\Pi_{el} = \int_0^\infty (P_T - P_N)dz \tag{3}$$

where P_T and P_N are the tangential and normal components of the Maxwell pressure tensor with respect to the interface. Equation 3 corresponds to integration of the excess tangential pressure along a semi-infinite plate of unit width, which is situated perpendicular to the interface (Figure 5a). In general, the Maxwell tensor, which expresses the pressure due to the electric field, has the form[41]

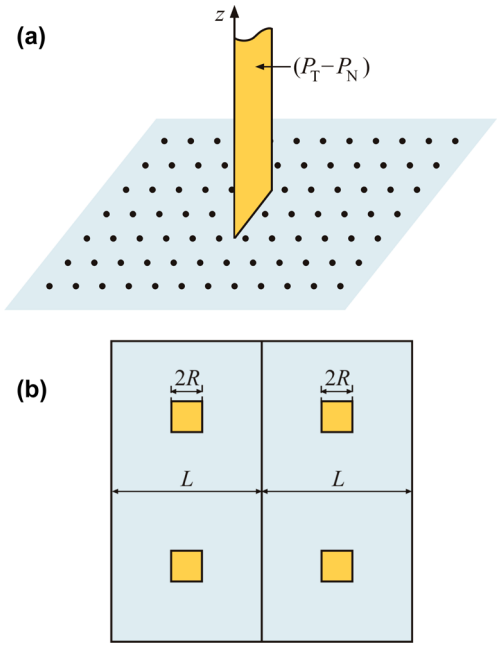

Figure 5. (a) Surface pressure due to a periodic surface charge distribution on the water/nonpolar-fluid interface can be calculated by integrating the excess Maxwell pressure, $P_T - P_N$, in accordance with the Bakker formula, eq 3, and averaging over one period, eq 6. (b) Cells of the periodic distribution can be modeled as squares of area L^2, equal to the actual mean area per particle, α, containing a square particle of side $2R$, where $R = 0.9306R_p$; see eq 26.

$$P_{ij} = \left(p_0 + \frac{\varepsilon_n}{8\pi}E^2\right)\delta_{ij} - \frac{\varepsilon_n}{4\pi}E_iE_j,\ \mathbf{E} \equiv -\nabla\psi \tag{4}$$

where δ_{ij} $(i,j = 1, 2, 3)$ is the Kronecker delta, ε_n is the dielectric constant of the nonpolar fluid, $\mathbf{E}$ and E_i denote the vector of the electric field and its component, ψ is the electrostatic potential, and p_0 is a background pressure.

From a mathematical viewpoint, the electric field created by the periodically distributed surface charges can be presented as a two-dimensional expansion in Fourier series. It is convenient to work with a square lattice (Figure 5b). The lattice is of period L and has the same area per particle as the real system. To calculate Π, we will take average values of the acting pressures over one period of the two-dimensional lattice. For this reason, the final result is not expected to be sensitive to the shape of the elementary cell, square or hexagon of the same area.

If the vertical plate in Figure 5a is oriented perpendicular to the x axis, from eq 4 we obtain

$$P_T - P_N = P_{xx} - P_{zz} = \frac{\varepsilon_n}{4\pi}\left[\left(\frac{\partial\psi}{\partial z}\right)^2 - \left(\frac{\partial\psi}{\partial x}\right)^2\right] \tag{5}$$

(Because of the symmetry of the system, the final result would be the same if the plate was oriented perpendicular to the y axis.) Then, the expression for the surface pressure acquires the form

$$\Pi_{el} \equiv \frac{1}{L^2}\int_{-L/2}^{L/2}dx\int_{-L/2}^{L/2}dy\int_0^\infty dz\frac{\varepsilon_n}{4\pi}\left[\left(\frac{\partial\psi}{\partial z}\right)^2 - \left(\frac{\partial\psi}{\partial x}\right)^2\right] \tag{6}$$

dx.doi.org/10.1021/la500126d | Langmuir 2014, 30, 2768−2778

Our next task is to find the potential $\psi(x,y,z)$, which obeys the Laplace equation in the nonpolar fluid

$$\frac{\partial^2\psi}{\partial x^2} + \frac{\partial^2\psi}{\partial y^2} + \frac{\partial^2\psi}{\partial z^2} = 0 \tag{7}$$

In view of Figure 5, the periodic surface charge, σ, can be expressed in the form

$$\frac{\sigma}{\sigma_{pn}} = \sum_{m=1}^{\infty} a_{m,0}\cos\left(m\pi\frac{2x}{L}\right) + \sum_{n=1}^{\infty} a_{0,n}\cos\left(n\pi\frac{2y}{L}\right) + \sum_{m,n=1}^{\infty} a_{m,n}\cos\left(m\pi\frac{2x}{L}\right)\cos\left(n\pi\frac{2y}{L}\right) \tag{8}$$

$a_{m,n}$ (m,n = 0, 1, 2 ...) are dimensionless coefficients, which can be determined if the function $\sigma(x,y)$ is specified; σ is scaled with the charge density at the particle/nonpolar-fluid interface, σ_{pn}. The boundary condition at the charged interface is

$$\frac{\partial\psi}{\partial z} = -\frac{4\pi}{\varepsilon_n}\sigma \text{ at } z = 0 \tag{9}$$

In view of eqs 8 and 9, the solution of eq 7 is

$$\psi = \sum_{m=1}^{\infty} A_{m,0}\cos\left(m\pi\frac{2x}{L}\right)\exp(-b_{m,0}z) + \sum_{n=1}^{\infty} A_{0,n}\cos\left(n\pi\frac{2y}{L}\right)\exp(-b_{0,n}z) + \sum_{m,n=1}^{\infty} A_{m,n}\cos\left(m\pi\frac{2x}{L}\right)\cos\left(n\pi\frac{2y}{L}\right)\exp(-b_{m,n}z) \tag{10}$$

where the coefficients are

$$b_{m,n} = \frac{2\pi}{L}(m^2 + n^2)^{1/2} \tag{11}$$

$$A_{m,n} = \frac{4\pi\sigma_{pn}}{\varepsilon_n}\frac{a_{m,n}}{b_{m,n}} \quad (m, n = 0, 1, 2, ...) \tag{12}$$

Substituting eq 10 into eq 6, after some transformations described in Appendix A, Supporting Information, we obtain

$$\Pi_{el} = \frac{\sigma_{pn}^2 L}{2\varepsilon_n}\left(\sum_{m=1}^{\infty}\frac{a_{0,m}^2}{m} + \frac{1}{2}\sum_{m,n=1}^{\infty}\frac{m^2 a_{m,n}^2}{(m^2+n^2)^{3/2}}\right) \tag{13}$$

Equation 13 expresses the electrostatic surface pressure for any periodic distribution of the surface charges, $\sigma(x,y)$, described by eq 8. The next step is to specify $\sigma(x,y)$ and determine the coefficients $a_{m,n}$.

4.3. Cell Model of the Surface Charge Distribution. When calculating electrostatic interactions across the nonpolar fluid between charged particles located at a liquid interface, a very good approximation is to assume that the electric field does not penetrate in the aqueous phase.[39] The reason is the considerably greater dielectric constant of water and the fact that the aqueous phase always contains ions. Then, in accordance with the boundary condition $\varepsilon_n E_n|_{z=0} = 4\pi\sigma$, each line of the electric field, emanating from a charge at the particle/nonpolar-fluid interface, ends at an oppositely charged effective counterion at the liquid interface, as sketched in Figure 6a. Here, we assume that the charges fixed at the particle/nonpolar fluid interface have a uniform density, σ_{pn}, whereas

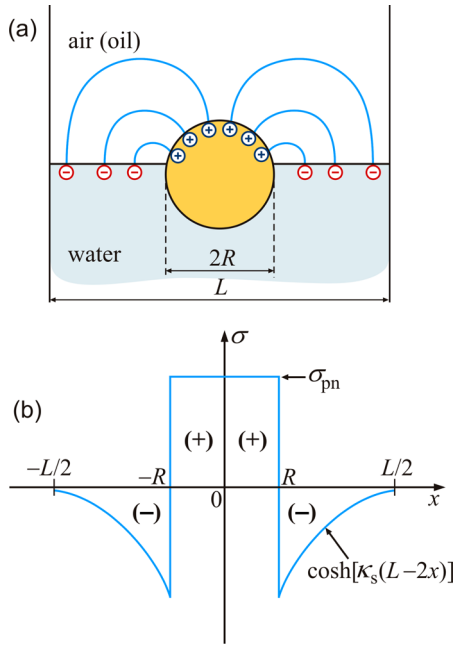

Figure 6. (a) Surface pressure due to a periodic surface charge distribution on the water/nonpolar-fluid interface can be calculated by integrating the excess Maxwell pressure, $P_T - P_N$, in accordance with the Bakker formula, eq 3, and averaging over one period, eq 6. (b) Cells of the periodic distribution can be modeled as squares of area L^2, equal to the actual mean area per particle, α, containing a square particle of side $2R$, where $R = 0.9306R_p$; see eq 26.

the free counterions on the liquid interface may have a nonuniform distribution, because they are attracted by the oppositely charged particle. As illustrated in Figure 5b, the particles are modeled as squares of side $2R$, whereas a qualitative picture of the surface charge distribution within a cell of the periodical surface lattice is shown in Figure 6b. As already mentioned, the differences between the real (rounded) and the model (square) particle shape is not so essential in view of the averaging in eq 6. In addition, the charge distribution in Figure 6a implies that the net charge within an interfacial cell must be zero

$$\int_{-L/2}^{L/2} dx \int_{-L/2}^{L/2} dy\sigma(x, y) = 0 \tag{14}$$

Note that $\sigma(x,y)$ defined by eq 8 satisfies eq 14. Equation 14 corresponds to a *cell model*, i.e., all counterions of a given particle are contained in an elementary cell of area L^2. This is one of the main differences with the model with discrete dipoles,[3] where the counterions of a given particle are distributed over the whole liquid interface.

As demonstrated in Appendix A, Supporting Information, the above requirements are satisfied by the following model expression for $\sigma(x,y)$

$$\frac{\sigma(x, y)}{\sigma_{pn}} = \frac{g_0^2}{g_0^2 - \xi^2}f(x)f(y) - \frac{\xi^2}{g_0^2 - \xi^2}g(x)g(y) \tag{15}$$

where $\xi = 2R/L$ and $f(x)$ is a stepwise function

$$f(x) = \begin{cases} 1 \text{ for } |x| \le R \\ 0 \text{ for } R < |x| \le L/2 \end{cases} \tag{16}$$

g is a continuous even function of x that satisfies the relations

dx.doi.org/10.1021/la500126d | Langmuir 2014, 30, 2768−2778

$$g(x) = 1 \text{ for } |x| \le R \text{ and } \frac{dg}{dx} = 0 \text{ for } |x| = \frac{L}{2} \quad (17)$$

The Fourier series expansion of $g(x)$ reads

$$g(x) = g_0 + \sum_{n=1}^{\infty} g_n \cos\left(n\pi\frac{2x}{L}\right) \quad (18)$$

The coefficient g_0 in eq 18 is the same quantity that takes part in eq 15. First, we will work with $g(x)$ expressed as a Fourier series (eq 18), and subsequently, the coefficients in this series will be determined.

The coefficients in eq 15 have been determined in such a way that the electroneutrality condition of the cell model, eq 14, is satisfied; see Appendix A, Supporting Information. Expanding eq 15 in Fourier series and comparing with eq 8 we find the coefficients in eq 13

$$a_{m,0} = a_{0,m} = \frac{f_0 g_0}{g_0^2 - f_0^2}(g_0 f_m - f_0 g_m) \quad (19)$$

$$a_{m,n} = \frac{g_0^2 f_m f_n - f_0^2 g_m g_n}{g_0^2 - f_0^2} \ (m, n = 1, 2, \ldots) \quad (20)$$

where f_n ($n = 0, 1, 2, \ldots$) are the coefficients in the Fourier series expansion of the function $f(x)$ defined by eq 16

$$f_0 = \xi, f_n = \frac{2}{n\pi}\sin(n\pi\xi) \ (n = 1, 2, \ldots) \quad (21)$$

Finally, we have to introduce a model expression for the distribution of the counterions on the water/nonpolar-fluid interface around the particle; see Figure 6a. In other words, we have to specify the form of the function $g(x)$ at $R < x \le L/2$. A definition of $g(x)$, which is compatible with eqs 17 and 18, is as follows

$$g(x) = \frac{\cosh[\kappa_s(L - 2|x|)]}{\cosh[\kappa_s(L - 2R)]} \text{ for } R < |x| \le \frac{L}{2} \quad (22)$$

This model expression for $g(x)$ corresponds to a decrease of the counterion surface concentration with the distance from the charged particle (Figure 6b). Moreover, $g(x)$ has a minimum in the middle between two neighboring particles, as it must be. The characteristic decay length κ_s^{-1} is to be determined as an adjustable parameter when comparing the model with experimental surface pressure isotherms.

Using eqs 17 and 22, we determine the coefficients in eq 18

$$g_0 = \xi + \frac{\xi}{\kappa_d}\tanh\left(\frac{1 - \xi}{\xi}\kappa_d\right), \ \kappa_d \equiv 2\kappa_s R \quad (23)$$

$$g_n = \frac{2\kappa_d^2[\sin(n\pi\xi) + n\pi(g_0 - \xi)\cos(n\pi\xi)]}{n\pi(n^2\pi^2\xi^2 + \kappa_d^2)} \quad (24)$$

where κ_d is a dimensionless screening parameter; see Appendix A, Supporting Information, for details.

Now, the model surface pressure isotherm is completely determined: Π_{el} is defined as a function of the dimensionless interparticle distance $\xi^{-1} = L/(2R)$ by eq 13, along with eqs 19, 20, 21, 23, and 24. The dependence of the dimensionless surface pressure $\varepsilon_n\Pi_{el}/(R\sigma_{pn}^2)$ on ξ is a universal function, which depends on a single parameter, κ_d. This dependence is plotted in Figure 7 for four different values of κ_d. The results show that the dimensionless surface pressure is not so sensitive

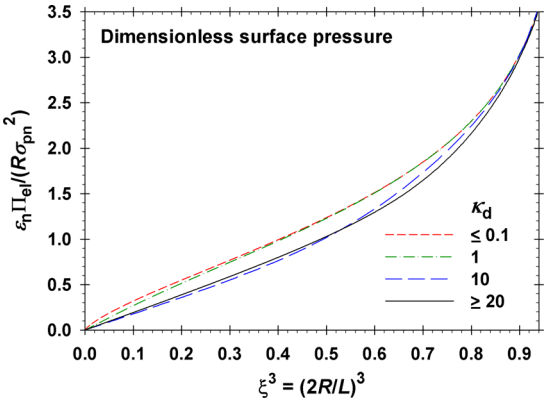

Figure 7. Plot of the dimensionless electrostatic surface pressure $\varepsilon_n\Pi_{el}/(R\sigma_{pn}^2)$ vs ξ^3 for four values of κ_d denoted in the figure. At $\kappa_d \le 0.1$ the calculated curves coincide with the uppermost dashed line, whereas at $\kappa_d \ge 20$ the calculated curves coincide with the solid line.

to the value of κ_d. For $\kappa_d \le 0.1$ the isotherms coincide with the upper curve in Figure 7, whereas at $\kappa_d > 20$ the isotherms coincide with the curve with $\kappa_d = 20$ in the same figure. Remarkably, the curve with $\kappa_d \ge 20$ in Figure 7 has a long linear portion at the lower values of the surface pressure, in agreement with the experimental data in Figure 3b and 3c. This curve is tabulated in Appendix A, Supporting Information (see Table S1 therein). In the next section, the experimental data are fitted with the model at fixed $\kappa_d = 20$ using σ_{pn} in eq 13 as an adjustable parameter.

4.4. Comparison of the Theoretical Model with Experimental Data. The side L of the square cell (see Figures 5 and 6) can be defined as follows

$$L = 2R\left(\frac{A}{A_h}\right)^{1/2} \quad (25)$$

At close packing, $A/A_h = 1$, eq 25 yields $L = 2R$, as it must be; see Figure 5b. In view of the relation $\alpha = L^2$, substitution of A/A_h from eq 2 into eq 25 yields the following relation between the model's parameter R and the particle radius R_p

$$R = (0.5\sqrt{3})^{1/2}R_p \approx 0.9306R_p \quad (26)$$

Assuming that the electric field in the real system is due to charges at the particle/nonpolar-fluid interface with surface density σ, we can set equal the particle charges in the real and model systems

$$2\pi R_p^2(1 - \cos\theta)\sigma = (2R)^2\sigma_{pn} \quad (27)$$

Equation 27 can be used to determine the real surface charge density, σ, from the value of σ_{pn} obtained from the data fit if the particle contact angle θ is known. Finally, in view of eq 1, the experimental surface pressure Π and the theoretical electrostatic component of surface pressure, Π_{el}, are related as follows

$$\Pi = \Pi_{el} - \Pi_0 \quad (28)$$

where Π_0 is an additive constant that is to be determined from the fit.

All theoretical curves in Figures 8 and 9 are drawn with a fixed $\kappa_d = 20$, whereas σ_{pn} and Π_0 are determined as adjustable parameters from the fits; the obtained values are shown in the respective figures. Figure 8a shows one of the experimental surface pressure isotherms in Figure 3b; the full circles are the

dx.doi.org/10.1021/la500126d | Langmuir 2014, 30, 2768−2778

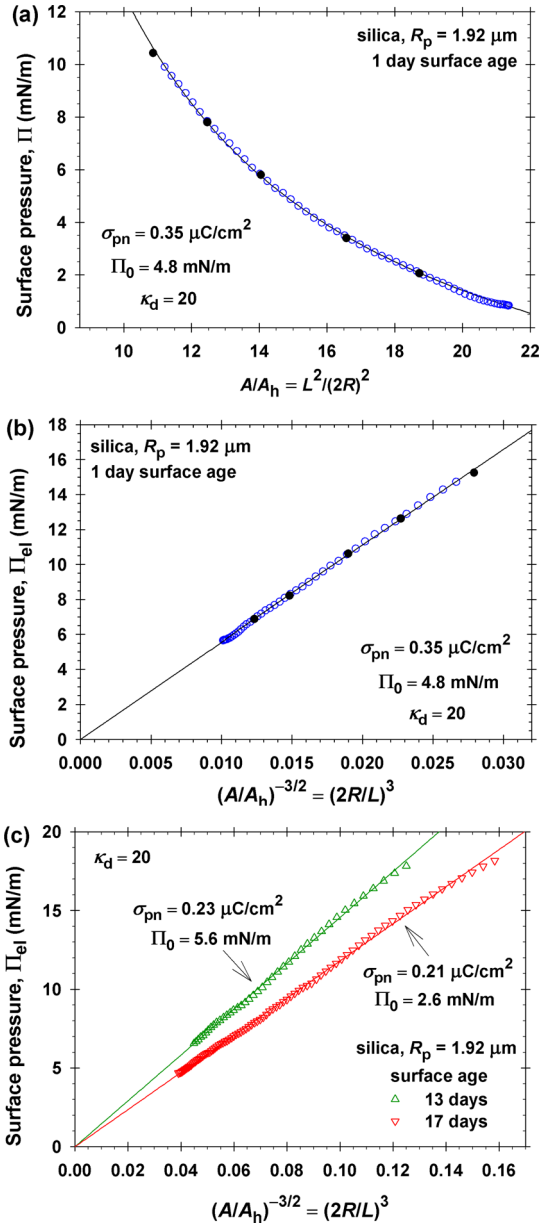

Figure 8. Our data for the surface pressure (the points) and respective best fits with the theoretical model (the lines). (a) Plot of Π vs A/A_h for particles of 1 day surface age. (b) Same data plotted as Π_{el} vs $(A/A_h)^{-3/2}$. (c) Plots of Π_{el} vs $(A/A_h)^{-3/2}$ for particles of 13 and 17 days surface age. Values of σ_{pn} and Π_0 determined from the fits are shown in the figure.

separate points in Figure 3b at which video frames have been processed to determine N. There is an excellent agreement between the data and the theoretical curve. In Figure 8b, the same data are plotted as Π_{el} vs $(2R/L)^3$. The obtained linear dependence indicates that the whole set of experimental data belongs to the asymptotic region where $\Pi_{el} \propto L^{-3}$. The additive constant Π_0 has been determined in such a way that the straight line in Figure 8b passes through the coordinate origin.

Figure 8c shows similar plots of data for monolayers from silica particles that have been stored for 13 and 17 days in isopropyl alcohol before the experiment. The slopes of the plots are considerably smaller than those in Figure 8b and correspond to smaller values of σ_{pn} determined from the fit, which are shown in the figure. The results indicate a considerable decrease of the particle surface charge upon storage in isopropyl alcohol (IPA). Because $\Pi_{el} \propto \sigma_{pn}^2$, see eq 13, a 2-fold decrease in the surface charge density leads to a decrease in the surface pressure with a factor of 4.

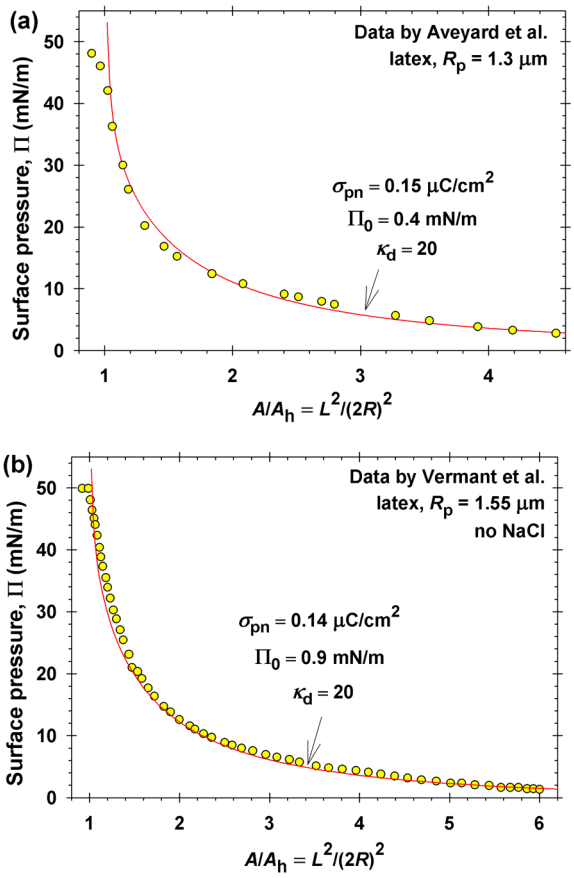

Figure 9. Experimental data for Π vs A/A_h (the points) and respective best fits with the theoretical model (the lines). (a) Data by Aveyard et al.[3] (b) Data by Vermant et al.[20] Values of σ_{pn} and Π_0 determined from the fits are shown in the figure.

Our experiments indicate that the particles are negatively charged after drying in the end of the hydrophobization procedure (see above). The decrease of their charge during storage in IPA could be explained with desorption of ions bound to the particle surfaces, which is facilitated by the relatively high relative dielectric constant of IPA, ε = 18.6 at 25 °C.

Figure 9a and 9b shows a comparison of the model with literature data[3,20] for the surface pressure of monolayers from latex particles at oil/water interfaces. In this case, the experimental data include the whole range of interparticle distances, both the asymptotic region with $\Pi_{el} \propto L^{-3}$ and the region near collapse, $A/A_h \to 1$. The agreement of the model with the experimental data is excellent at all degrees of monolayer compression.

The results for the model's parameter σ_{pn} in Figures 8 and 9 are compared in Table 1. The fourth column shows the values of the real surface charge density, σ, estimated from eq 27, along with eq 26. For this estimate, values of the contact angle obtained in the respective studies were used, viz. θ = 85.4°, 80°, and 130° for the data from Figures 8, 9a, and 9b, respectively. For the latex particles, the surface densities of ionizable groups are known, 7.7 and 9.1 μC/cm^2 for Figures 9a and 9b, respectively.[3,20] The values of σ in Table 1 for these two

dx.doi.org/10.1021/la500126d | Langmuir 2014, 30, 2768−2778

Table 1. Surface Charges Determined from Fits of Surface Pressure Isotherms

data from	material	σ_{pn} (μC/cm^2)	σ (μC/cm^2)	specific area (nm^2/charge)
Figure 8a, 1 day age	silica	0.35	0.21	76.2
Figure 8c, 13 days age	silica	0.23	0.14	116
Figure 8c, 17 days age	silica	0.21	0.12	129
Figure 9a	latex	0.15	0.10	160
Figure 9b	latex	0.14	0.047	342

experiments correspond to ionization degrees α = 1.3% and 0.52%, which are not so different from the values α = 1.03% and 0.33% determined in refs 3 and 20 by means of fits with a different model.

The developed theoretical approach refers to electric charges of surface density σ located at the particle/nonpolar-fluid interface. However, this approach is applicable also if the electric field in the nonpolar fluid is due to electric charges of density σ_{pw} located at the particle/water interface. In the nonpolar fluid, such charges create the same electric field as charges of density

$$\sigma = \frac{\varepsilon_n(1 + \cos\theta)}{\varepsilon_w \kappa R_p D \sin^3\theta}\sigma_{pw} \quad (29)$$

located at the particle/nonpolar-fluid interface. Here, κ is the Debye screening parameter in the aqueous phase, $D = D(\theta,\varepsilon_{pn})$ is a known dimensionless function, which can be calculated by means of Table 1 and eq D.1 in ref 42, $\varepsilon_{pn} \equiv \varepsilon_p/\varepsilon_n$ is the ratio of the dielectric constants of the particle and nonpolar fluid, and ε_w is the dielectric constant of water. Equation 29 is obtained by setting equal the effective particle dipole moments, p_d, due to charges at the particle/water and particle/nonpolar-fluid interfaces; see eqs 1.2 and 1.3 in ref 39. To calculate Π_{el}, the charge density estimated from eq 29 is to be summed up with the real charge density at the particle/nonpolar-fluid interface (if any). Equation 29 shows that the contribution of σ_{pw} decreases with the rise of both the particle radius R_p and the salt concentration in the water phase (via κ).

The fact that the data in Figures 8 and 9 have been fitted with the theoretical curve at κ_d = 20 (see Figure 7) calls for discussion. As already mentioned, at $\kappa_d \geq 20$ the theoretical curves coincide and exhibit a long asymptotic region where $\Pi_{el} \propto L^{-3}$. (The latter was the reason to choose κ_d = 20 for the fits). $\kappa_d \geq 20$ corresponds to $\kappa_s^{-1} \leq 0.1\ R$ and means that the effective counterions on the liquid interface (see Figure 6a) are concentrated in the close vicinity of the charged particles, which is compatible with the expectation for dipolar character of the field at long distances.[17,18]

5. SUMMARY AND CONCLUSIONS

In the present work, we investigate nondensely packed spread monolayers of electrically charged micrometer-sized silica particles on the air/water interface. The electrostatic repulsion between the particles occurs through the air phase. Surface pressure vs area isotherms were measured by Langmuir trough, and the monolayers' morphology was monitored by microscope. The mean area per particle is determined by Delaunay triangulation and Voronoi diagrams. In terms of mean area, the surface pressure for monolayers from polydisperse particles obeys the same law as for monodisperse particles. The experiments indicate that at large interparticle separations this law reduces to $\Pi \propto L^{-3}$. A theoretical cell model is developed, which predicts the aforementioned asymptotic law. The model presumes a periodic distribution of the surface charge density, which induces a corresponding electric field in the air phase. Then, the Maxwell pressure tensor of the electric field is calculated and integrated according to Bakker's formula to find the surface pressure, Π, which is obtained in the form of a Fourier series. Thus, all collective effects from the electrostatic interparticle interactions are taken into account. The model considers particles of finite size, so that the excluded area effects are also taken into account. It excellently agrees with experimental data obtained by us and other authors[3,20] in the whole range of interparticle separations, not only at large L. In all investigated cases, the variations in Π upon compression or expansion of the particulate monolayer are completely dominated by the electrostatic interactions, the entropic contribution in Π being negligible.

By evaporation of the water in a Langmuir minitrough, the particle monolayers have been deposited on a solid substrate placed on the bottom of the trough. The electrostatic interparticle repulsion is preserved during the whole deposition process. This repulsion is strong enough to withstand the attractive lateral capillary immersion forces that are operative during the final stage of drying of the particle monolayer on the substrate.[29,36] The capillary forces cause only a slight shrinking of the layer, within ca. 17%.

The obtained experimental results and the developed theoretical model could be useful for prediction and control of the properties of nondensely packed interfacial monolayers from charged particles, which are utilized for producing micropatterned surfaces with wide potential applications.[4−10]

■ ASSOCIATED CONTENT

Supporting Information

Appendix A (Additional results: determination of the mean area per particle), α; asymptotic behavior of literature data for $\Pi(A)$; model with a periodic surface charge density; cell model of the surface charge distribution; changes in the particle monolayer upon drying on a solid substrate; effect of salt; tabulated dimensionless function $F(\xi,20)$. This material is available free of charge via the Internet at http://pubs.acs.org.

■ AUTHOR INFORMATION

Corresponding Author

*Phone (+359) 2-8161262. Fax (+359) 2-9625643. E-mail: pk@lcpe.uni-sofia.bg.

Notes

The authors declare no competing financial interest.

■ ACKNOWLEDGMENTS

The authors gratefully acknowledge the support from the National Science Fund of Bulgaria, grant no. DO-02-121/2009, from the FP7 project Beyond-Everest, and from the ESF COST Action CM1101.

■ REFERENCES

(1) Schuller, H. Modellversuche zur Spreitung von Kolloid-Partikeln. *Kolloid Z. Z. Polym.* **1967**, *216*, 380−383.

(2) Sheppard, E.; Tcheurekdjian, N. Monolayer studies. IV. Surface films of emulsion latex particles. *J. Colloid Interface Sci.* **1968**, *28*, 481−486.

(3) Aveyard, R.; Clint, J. H.; Nees, D.; Paunov, V. N. Compression and structure of monolayers of charged latex particles at air/water and octane/water interfaces. *Langmuir* **2000**, *16*, 1969−1979.
(4) Ray, M. A.; Jia, L. Micropatterning by non-densely packed interfacial colloidal crystals. *Adv. Mater.* **2007**, *19*, 2020−2022.
(5) Zhao, Y.; Wang, J.; Mao, G. Colloidal subwavelength nanostructures for antireflection optical coatings. *Opt. Lett.* **2005**, *30*, 1885−1887.
(6) Min, W.-L.; Jiang, P.; Jiang, B. Large-scale assembly of colloidal nanoparticles and fabrication of periodic subwavelength structures. *Nanotechnology* **2008**, *19*, 475604.
(7) Cayre, O. J.; Paunov, V. N. Fabrication of microlens arrays by gel trapping of self-assembled particle monolayers at the decane−water interface. *J. Mater. Chem.* **2004**, *14*, 3300−3302.
(8) Sun, Y.; Forrest, S. R. Organic light emitting devices with enhanced outcoupling via microlenses fabricated by imprint lithography. *J. Appl. Phys.* **2006**, *100*, 073106.
(9) Isa, L.; Kumar, K.; Müller, M.; Grolig, J.; Textor, M.; Reimhult, E. Particle lithography from colloidal self-assembly at liquid−liquid interfaces. *ACS Nano* **2010**, *4*, 5665−5670.
(10) Bettinger, C. J.; Langer, R.; Borenstein, J. T. Engineering substrate micro- and nanotopography to control cell function. *Angew. Chem., Int. Ed.* **2009**, *48*, 5406−5415.
(11) Stancik, E. J.; Kouhkan, M.; Fuller, G. G. Coalescence of particle-laden fluid interfaces. *Langmuir* **2004**, *20*, 90−94.
(12) Horozov, T. S.; Aveyard, R.; Clint, J. H.; Neumann, B. Particle zips: vertical emulsion films with particle monolayers at their surfaces. *Langmuir* **2005**, *21*, 2330−2341.
(13) Monteux, C.; Jung, E.; Fuller, G. G. Mechanical properties and structure of particle coated interfaces: influence of particle size and bidisperse 2D suspensions. *Langmuir* **2007**, *23*, 3975−3980.
(14) Xu, H.; Kirkwood, J.; Lask, M.; Fuller, G. Charge interaction between particle-laden fluid interfaces. *Langmuir* **2010**, *26*, 3160−3164.
(15) Crossley, S.; Faria, J.; Shen, M.; Resasco, D. E. Solid nanoparticles that catalyze biofuel upgrade reactions at the water/oil interface. *Science* **2010**, *327*, 68−72.
(16) Garbin, V.; Crocker, J. C.; Stebe, K. J. Nanoparticles at fluid interfaces: Exploiting capping ligands to control adsorption, stability and dynamics. *J. Colloid Interface Sci.* **2012**, *387*, 1−11.
(17) Aveyard, R.; Binks, B. P.; Clint, J. H.; Fletcher, P. D. I.; Horozov, T. S.; Neumann, B.; Paunov, V. N.; Annesley, J.; Botchway, S. W.; Nees, D.; Parker, A. W.; Ward, A. D.; Burgess, A. N. Measurement of long-range repulsive forces between charged particles at an oil-water interface. *Phys. Rev. Lett.* **2002**, *88*, 246102.
(18) Park, B. J.; Pantina, J. P.; Furst, E. M.; Oettel, M.; Reynaert, S.; Vermant, J. Direct measurements of the effects of salt and surfactant on interaction forces between colloidal particles at water-oil interfaces. *Langmuir* **2008**, *24*, 1686−1694.
(19) Horozov, T. S.; Aveyard, R.; Clint, J. H.; Binks, B. P. Order-disorder transition in monolayers of modified monodisperse silica particles at the octane-water interface. *Langmuir* **2003**, *19*, 2822−2829.
(20) Reynaert, S.; Moldenaers, P.; Vermant, J. Control over colloidal aggregation in monolayers of latex particles at the oil-water interface. *Langmuir* **2006**, *22*, 4936−4945.
(21) Horozov, T. S; Binks, B. P. Particle behavior at horizontal and vertical fluid interfaces. *Colloids Surf., A* **2005**, *267*, 64−73.
(22) Masschaele, K.; Vermant, J. Electric field controlled capillary traps at water/oil interfaces. *Soft Matter* **2011**, *7*, 10597−10600.
(23) Pergamenshchik, V. M. Strong collective attraction in colloidal clusters on a liquid-air interface. *Phys. Rev., E* **2009**, *79*, 011407.
(24) Domínguez, A.; Oettel, M.; Dietrich, S. Dynamics of colloidal particles with capillary interactions. *Phys. Rev., E* **2010**, *82*, 011402.
(25) Ray, M. A.; Shewmon, N.; Bhawalkar, S.; Jia, L.; Yang, Y.; Daniels, E. S. Submicrometer surface patterning using interfacial colloidal particle self-assembly. *Langmuir* **2009**, *25*, 7265−7270.
(26) Ma, H.; Perea, B.; Dai, L. L. Study of two-component colloidal particles at air/water interfaces using Langmuir−Blodgett techniques. *Colloids Surf., A* **2010**, *372*, 61−65.
(27) Bhawalkar, S. P.; Qian, J.; Heiber, M. C.; Jia, L. Development of a colloidal lithography method for patterning nonplanar surfaces. *Langmuir* **2010**, *26*, 16662−16666.
(28) Hansen, P. H. F.; Rödner, S.; Bergström, L. Structural characterization of dense colloidal films using a modified pair distribution and Delaunay triangulation. *Langmuir* **2001**, *17*, 4867−4875.
(29) Kralchevsky, P. A.; Nagayama, K. Capillary forces between colloidal particles. *Langmuir* **1994**, *10*, 23−36.
(30) Christov, N. C.; Danov, K. D.; Danova, D. K.; Kralchevsky, P. A. The drop size in membrane emulsification determined from the balance of capillary and hydrodynamic forces. *Langmuir* **2008**, *24*, 1397−1410.
(31) Marinova, K. G.; Christova, D.; Tcholakova, S.; Efremov, E.; Denkov, N. D. Hydrophobization of glass surface by adsorption of poly(dimethylsiloxane). *Langmuir* **2005**, *21*, 11729−11737.
(32) Boneva, M. P.; Christov, N. C.; Danov, K. D.; Kralchevsky, P. A. Effect of electric-field-induced capillary attraction on the motion of particles at an oil−water interface. *Phys. Chem. Chem. Phys.* **2007**, *9*, 6371−6384.
(33) Hansen, P. H. F.; Bergström, L. Perikinetic aggregation of alkoxylated silica particles in two dimensions. *J. Colloid Interface Sci.* **1999**, *218*, 77−87.
(34) Kolarž, P. M.; Filipović, D. M.; Marinković, B. P. Daily variations of indoor air-ion and radon concentrations. *Appl. Radiat. Isot.* **2009**, *67*, 2062−2067.
(35) Garbin, V.; Crocker, J. C.; Stebe, K. J. Forced desorption of nanoparticles from an oil-water interface. *Langmuir* **2012**, *28*, 1663−1667.
(36) Denkov, N. D.; Velev, O. D.; Kralchevsky, P. A.; Ivanov, I. B.; Yoshimura, H.; Nagayama, K. Mechanism of formation of two-dimensional crystals from latex particles on substrates. *Langmuir* **1992**, *8*, 3183−3190.
(37) Hurd, A. J. The electrostatic interaction between interfacial colloidal particles. *J. Phys. A: Math. Gen.* **1985**, *18*, L1055−L1060.
(38) Oettel, M.; Dietrich, S. Colloidal interactions at fluid interfaces. *Langmuir* **2008**, *24*, 1425−1441.
(39) Danov, K. D.; Kralchevsky, P. A. Interaction between like-charged particles at a liquid interface: Electrostatic repulsion vs. electrocapillary attraction. *J. Colloid Interface Sci.* **2010**, *345*, 505−514.
(40) Bakker, G. Kapillarität und Oberflächenspannung. In *Handbuch der Experimentalphysik*, Band 6; Akademische Verlagsgesellschaft: Leipzig, 1928.
(41) Landau, L. D.; Pitaevskii, L. P.; Lifshitz, E. M. *Electrodynamics of Continuous Media*, 2nd ed.; Butterworth-Heinemann, Oxford, 1984; Vol. *8* (Course of Theoretical Physics).
(42) Danov, K. D.; Kralchevsky, P. A. Electric forces induced by a charged colloid particle attached to the water−nonpolar fluid interface. *J. Colloid Interface Sci.* **2006**, *298*, 213−231.